PAPER

Electric field tuning non-volatile dynamic magnetism in half-metallic alloys $Co_2FeAl/Pb(Mg_{1/3}Nb_{2/3})O_3$-$PbTiO_3$ heterostructure

To cite this article: Gesang Dunzhu *et al* 2019 *Mater. Res. Express* **6** 066114

Materials Research Express

PAPER

Electric field tuning non-volatile dynamic magnetism in half-metallic alloys $Co_2FeAl/Pb(Mg_{1/3}Nb_{2/3})O_3$-$PbTiO_3$ heterostructure

Gesang Dunzhu[1,3], **Fufu Liu**[1,3], **Yangping Wang**[1,3], **Cai Zhou**[2,4] **and Changjun Jiang**[1,3,4]

[1] Key Laboratory for Magnetism and Magnetic Materials of MOE, Lanzhou University, Lanzhou 730000, People's Republic of China
[2] Hubei Province Engineering Research Center for Intelligent Micro-nano Medical Equipment and Key Technologies, School of Electrical and Electronics Engineering, No. 1 sunshine Avenue, Jiangxia District, Wuhan, People's Republic of China
[3] Key Laboratory of Special Function Materials and Structure Design, Ministry of Education, Lanzhou University, Lanzhou 730000, People's Republic of China
[4] Authors to whom any correspondence should be addressed.

E-mail: szhou@wtu.edu.cn **and** jiangchj@lzu.edu.cn

RECEIVED
11 January 2019

REVISED
10 February 2019

ACCEPTED FOR PUBLICATION
13 March 2019

PUBLISHED
29 March 2019

Keywords: half-metallic, $Co_2FeAl/Pb(Mg_{1/3}Nb_{2/3})O_3$-$PbTiO_3$ heterostructures, dynamic magnetic property, non-volatile

Abstract

The half-metallic characteristic of Co_2FeAl Huesler alloy films in $Co_2FeAl/Pb(Mg_{1/3}Nb_{2/3})O_3$-$PbTiO_3$ heterostructure was controlled by different substrate temperatures during deposition. The evolution of microstructure shows the *B*2 ordering degree of Co_2FeAl thin film increase with the substrate temperature decreasing from 550 °C to 480 °C during deposition, which can be verified by anisotropy magnetoresistance measurement. Moreover, the result measured by rotating-angle ferromagnetic resonance demonstrates *B*2 ordering degree of Co_2FeAl thin film controlled the change of symmetry of magnetic anisotropy. In addition, the *loop*-like curve of magnetic resonance field/linewidth versus electric field exhibits the non-volatile behavior, which can be attributed to the 109° ferroelectric domain switching of PMN-PT substrate. This result can provide opportunities for magnetization control in multiferroic devices.

Introduction

Half-metallic materials, have triggered great attention because of the perfect spin polarization of conduction electrons at the Fermi level, which is used to enhance the spin-dependent transport efficiency of high performance spintronic device [1–6]. Among half-metallic materials, Co-based Heusler alloys, such as Co_2FeAl, generally with a low magnetic damping constant and a high Currie temperature became a hot spot in this field. The material Co_2FeAl (CFA) has the composition X_2YZ (where X and Y are the different transition metal elements, and Z is a group III, IV, or V element) [7–9]. According to the variety of derived structure types originating from atomic order degree in the occupation of the available sites, three different phases of CFA thin film obtained. $L2_1$ phase with totally order degree is difficult to achieve. *B*2 phase is with X atoms occupying their assigned sites, while Y and Z atoms randomly sharing the other ones, and *A*2 phase with a completely random occupation for any X, Y, or Z atom. On the other hand, a complete disorder among occupation for X, Y, or Z atom leads to a further reduction of the crystal symmetry to the *A*2 phase [10–12]. For sample measurement, except for the CFA's fundamental peak measured by x-ray diffraction (XRD), the negative anisotropy magnetoresistance (AMR) ratio can also be a fingerprint for half-metallic material [13–15]. For sample preparation, these factors, which can influence atomic ordering degree, half-metallic and magnetic character related to the *d* orbital electrons of CFA, include sample preparation methods, the annealing temperature after deposition, different substrates, and especially different substrate temperatures during deposition. Considering the continuing development of many existing and emerging devices such as magnetoresistive random access memory, the manipulation of magnetization using electric fields in ferromagnetic/ferroelectric (FM/FE) heterostructures has sparked intensive research because of the accuracy and accessibility of the method, which represents a pathway towards lower dynamic energy dissipation [16–20]. One particular ferroelectric crystal substarte $Pb(Mg_{1/3}Nb_{2/3})O_3$-$PbTiO_3$ (PMN-PT) is often used in FM/FE heterostructure to manipulate the

magnetic anisotropy of the adjacent magnetic layer, which results in a magnetoelectric (ME) effect [21–24]. In our previous reports, we have investigated piezostrain induced by electric field controlling magnetic anisotropy and the non-volatile electric field-based control of magnetic anisotropy in CFA/PMN-PT heterostructures only at room temperature [25, 26]. Therefore, in this work, we investigate in details the characteristic of CFA Huesler alloy films in CFA/PMN-PT heterostructure by changing substrate temperatures during deposition. The *B*2 ordering degree of CFA thin film change with the substrate temperature (T_s) decreasing from 550 °C to 480 °C during deposition, which can be verified by XRD and dynamic magnetic measurements. Moreover, the non-volatile behavior of resonance-magnetic-field/linewidth versus electric field (*E*) can be obtained in CFA/PMNPT heterostructure at 480 °C, which can be attributed to the 109° ferroelectric domain switching of PMN-PT substrate [27–29].

Experimental procedure

The CFA thin film was deposited on the (001)-oriented PMN-PT substrate by direct current (DC) magnetron sputtering at different T_s 480 °C, 500 °C, 520 °C, and 550 °C, respectively. The sputtering condition includes Ar pressure of 0.1 Pa and flow rate at 10 SCCM (SCCM denotes cubic centimeter per minute at STP), with a base pressure of 2×10^{-5} Pa. The thickness of CFA thin films was all 150 nm. The Pt layers were sputtered as electrodes. The thickness of top and bottom Pt layer were 10 nm and 50 nm, respectively. Cu wires were connected on the electrodes by the adhesive tape. Keithley 2400 source measurement unit was used to test the resistance of the sample using the four-probe technique. XRD measurement was performed on X'Pert x-ray powder diffractometer with Cu K_α radiation (1.540 56 Å). The DC power supply (Keithley 2410) was used to provide biased voltage. Ferromagnetic resonance (FMR) measurements were performed on the JEOL, JES-FA 300 (X-band at 8.969 GHz) spectrometer. Moreover, considering the possible existence of ferroelastic domain switching, the piezoresponse force microscopy (PFM) images of the PMN-PT substrate were measured to understand the evolution of ferroelectric domain switching more clearly. All the results were measured at room temperature.

Results and discussion

The XRD patterns of the CFA films at different T_s during deposition were shown in figure 1(a). At room temperature, there was no peak corresponding to CFA phase detected in XRD scans. When increasing temperature to 480 °C, except for the peaks of PMN-PT substrate, (004) fundamental peak was observed at ~65.09° in this film, which is originated from the basic cubic crystal structure, corresponding to the *A*2 phase of CFA. The *A*2 phase was totally disordered with respect to Fe, Al, and Co. The presence of (002) peak at ~31.19° indicated that the sample contains *B*2 phase. The *B*2 phase is characterized by total disorder between Fe and Al atoms while Co atoms occupy regular sites [30, 31]. The similar behavior can be obtained at 500 °C, 520 °C, and 550 °C, respectively, which suggest the appearance of *B*2 phase. However, with the accuracy of the measurements, the $L2_1$-type peak at approximate 27 degree cannot be observed. The presence of the (002) and (004) peak for the CFA thin film grown on the (001)-oriented PMN-PT indicated that the thin films are textured. The integrated intensity ratio of (002) to (004) peak ($I_{(002)}/I_{(004)}$) as shown in the left of figure 1(b) increased with decreasing T_s from 550 °C to 480 °C, which demonstrated the improvement of the *B*2 phase ordering degree. Moreover, to quantify the chemical ordering of *B*2 phase, the parameter (S_{B2}) is given as following [32]:

$$\frac{I_{(200)}}{I_{(400)}} = S_{B2}^2 \left(\frac{I_{(200)}^{full-order}}{I_{(400)}^{full-order}} \right) \tag{1}$$

where $I_{(002)}/I_{(004)}$ is the ratio of the integrated intensity of the (002) peak to that of the (004) peak as determined by experiments, and $I_{(200)}{}^{\text{full-order}}/I_{(400)}{}^{\text{full-order}}$ is the ideal ratio of the two peaks. The dependence of the S_{B2} parameter on T_s was shown in the right of figure 2(b). The S_{B2} parameter increased from 32.6% to 43.3% with T_s decreasing from 550 °C to 480 °C. These results indicated highest ordered CFA films in this work can be achieved at 480 °C, which might be interpreted qualitatively as following: when the substrate temperature excess critical point, the continuing increase of ordering phase lead to the higher atom energy, which can be resulted to the increase of the atom disorder degree.

Except for the result measured by XRD, the anisotropy magnetoresistance (AMR) can also be a fingerprint for half-metallic/non-half-metallic material [15, 33]. AMR at different T_s were measured by electric transport measurement system. The experiment setup was shown in figure 2(a). The current 0.8 mA and magnetic field 1000 Oe were applied in the measurement process. The $[(\rho(\theta) - \rho_\perp)/\rho_\perp] \times 100\%$ of the CFA thin film as a function of θ (the direction of in-plane applied magnetic field *H* with respect to the [100] direction) can be

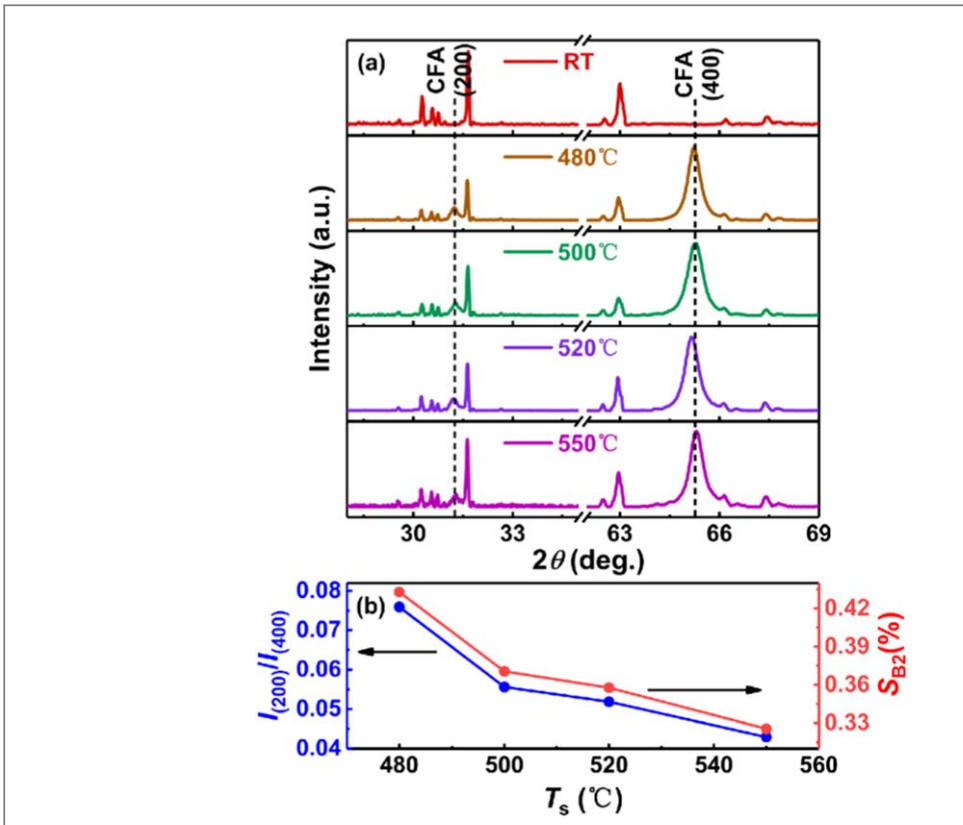

Figure 1. (a) XRD patterns of CFA/PMN-PT heterostructure at different T_s. (b) The dependence of T_s on $I_{(200)}/I_{(400)}$ and S_{B2}.

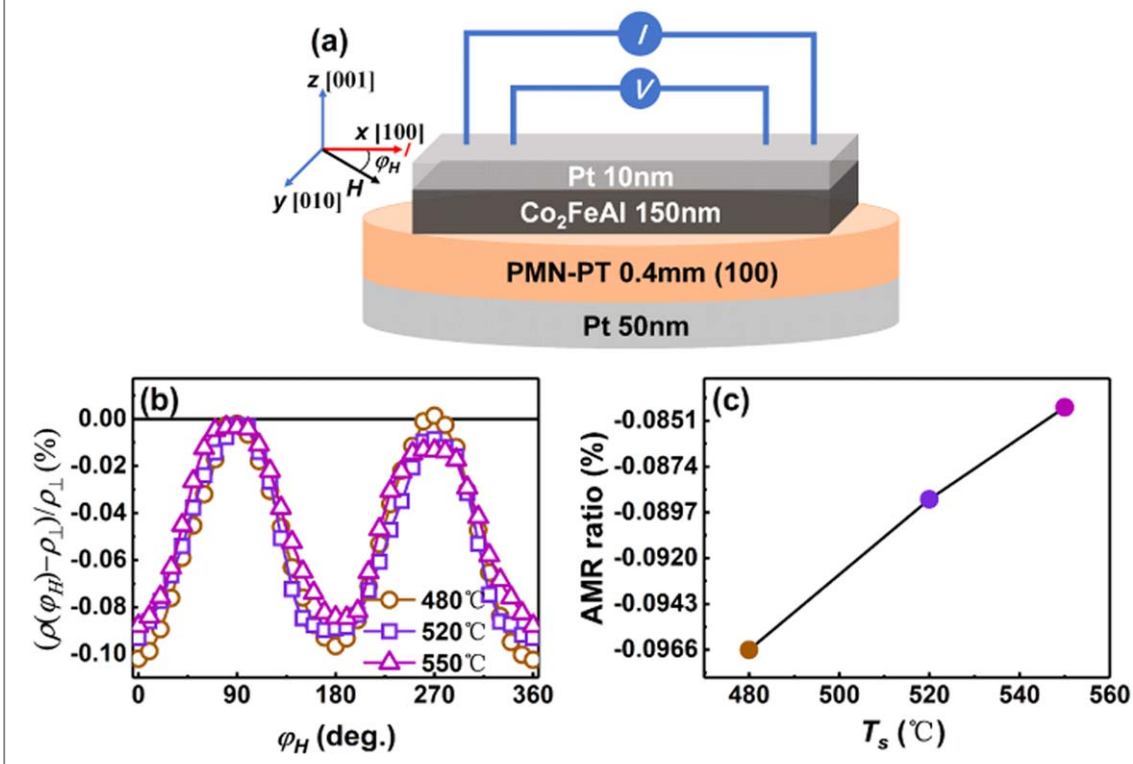

Figure 2. (a) Schematic diagram of AMR measurement. (b) $[(\rho(\theta) - \rho_\perp)/\rho_\perp] \times 100\%$ as a function of the angle between the magnetic field and applied current direction at 480 °C, 520 °C, and 550 °C. (c) AMR ratio (defined as $[(\rho_{//} - \rho_\perp)/\rho_\perp] \times 100\%$) with T_s changing from 480 °C to 550 °C.

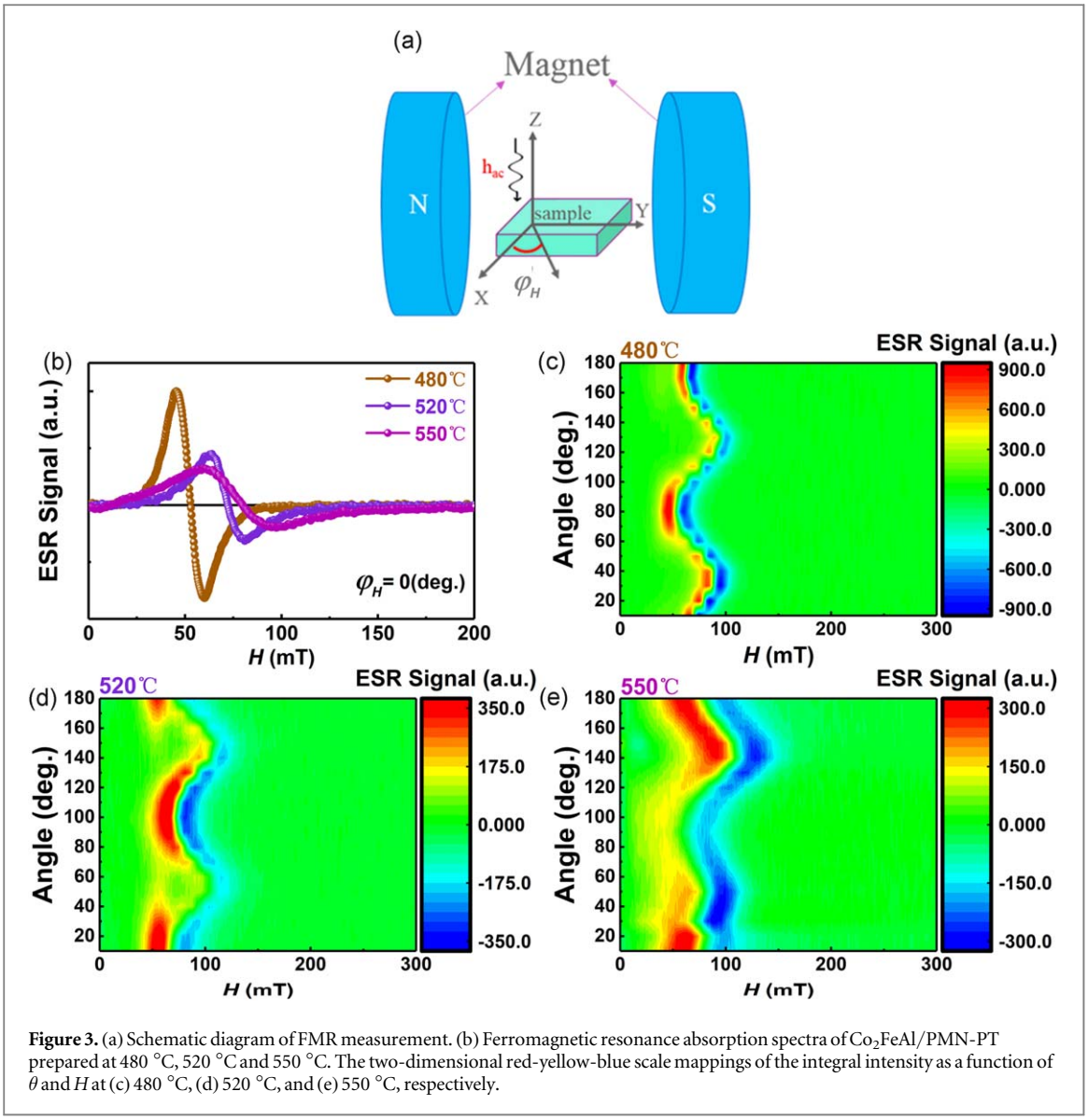

Figure 3. (a) Schematic diagram of FMR measurement. (b) Ferromagnetic resonance absorption spectra of Co_2FeAl/PMN-PT prepared at 480 °C, 520 °C and 550 °C. The two-dimensional red-yellow-blue scale mappings of the integral intensity as a function of θ and H at (c) 480 °C, (d) 520 °C, and (e) 550 °C, respectively.

obtained. The curve of $[(\rho(\theta) - \rho_\perp)/\rho_\perp] \times 100\%$ versus θ at different T_s were shown in figure 2(b), which showed the clear twofold symmetry. Generally, the sign of the $[(\rho(\theta) - \rho_\perp)/\rho_\perp] \times 100\%$ tend to be positive, which can be attributed to the dominant *s*-*d* scattering process is from up-spin *s*-state to down-spin *d*-states ($s\uparrow \rightarrow d\downarrow$) or $s\downarrow \rightarrow d\uparrow$. In contrast, as shown in figure 2(b), the $[(\rho(\theta) - \rho_\perp)/\rho_\perp] \times 100\%$ is negative due to the dominant scattering process $s\uparrow \rightarrow d\uparrow$ or $s\downarrow \rightarrow d\downarrow$, which was in agreement with that in Fe_4N and $Co_2Fe_xMn_{1-x}Si$ thin film. Therefore, the negative value of $[(\rho(\theta) - \rho_\perp)/\rho_\perp] \times 100\%$ was obtained, which can be proved the half-metallic of CFA thin film. Moreover, as shown in figure 2(c), with decreasing T_s, the increase of AMR ratio (defined as $[(\rho_{//} - \rho_\perp)/\rho_\perp] \times 100\%$) indicated the increase of *B*2 phase ordering degree, which was in consistent with the result measured by XRD.

In order to investigate the change of dynamic magnetic property induced by *B*2 phase ordering degree, the rotating-angle ferromagnetic resonance (FMR) spectra were measured. The schematic of FMR spectroscopy measurement was shown in figure 3(a). The measurement sample had a 1 mm × 1 mm square shape. The integral curves of FMR spectra under $\theta = 0°$ at T_s 480 °C, 520 °C, and 550 °C, respectively, were shown in figure 3(b). The linewidth had an obvious increase with increasing T_s. The two-dimensional red-yellow-blue scale mappings of the integral intensity as a function of θ and H at 480 °C, 520 °C, and 550 °C were shown in figures 3(c)–(e), respectively. In general, the magnetization is probed using a special phase correlation under the microwave excitation, and the FMR spectrum does not correspond to the imaginary part of the susceptibility alone, but in fact represents a mixture of the imaginary and real parts [34]. Therefore, the actual function of the absorption curve is given by an asymmetric Lorentzian function:

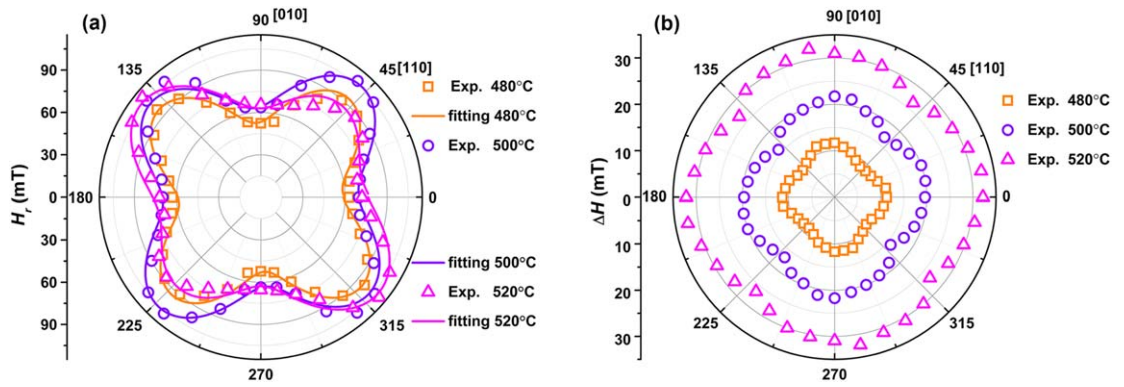

Figure 4. (a) The experimental results (dots) and fitting results (lines) of $H_r - \varphi_H$ at 480 °C, 520 °C, and 550 °C, respectively. (b) ΔH as a function of θ at 480 °C, 520 °C, and 550 °C, respectively.

$$\xi(H) = A\frac{\Delta H\cos\psi + (H - H_r)\sin\psi}{\Delta H^2 + (H - H_r)^2} \tag{2}$$

where A is the integral coefficient, ΔH is the half-width at half-maximum of the linewidth, H_r is the resonance field, ψ is the phase that mixes the real and imaginary parts of the dynamic susceptibility, and H is the external magnetic field. These integration curves of the FMR spectra were fitted using equation (2), and related parameters were obtained. At 480 °C, 520 °C, and 550 °C, the experimental dots of $H_r - \varphi_H$ can be obtained as shown in figure 4(a), which exhibited a superposition of two-fold and four-fold symmetric. The schematic of the established coordinate system in CFA/PMN-PT is shown in our previous report [35]. φ_H and φ_M are the angles of the in-plane applied field and the in-plane magnetization with respect to the start direction, respectively. θ_M is the angle of the out-of-plane magnetization with respect to the [001] direction. In this system, there exist many compete anisotropy energy including the magnetocrystalline anisotropy, in-plane uniaxial magnetic anisotropy energy, and magnetoelastic energy. Thereinto, the magnetoelastic energy and in-plane uniaxial magnetic anisotropy energy, which are both with two-fold symmetry, can be considered as the effective magnetic anisotropy energy. Therefore, the free energy on ferromagnetic resonance field [36] according to the Stoner-Wohlfarth model can be expressed as:

$$\begin{aligned} F = &-M_sH\sin\theta_M\cos(\varphi_M - \varphi_H) - 2\pi M_s^2\sin^2\theta_M - \frac{1}{8}K_{4//}\sin^2\theta_M(3 + 4\cos 4\varphi_H) \\ &- K_{eff}\sin^2\theta_M\sin^2\varphi_H \end{aligned} \tag{3}$$

Here, the first term is the external magnetic field energy, the second term is the demagnetizing energy, the third term is the magnetocrystalline anisotropy energy, the remaining one is the effective magnetic anisotropy energy. Furthermore, K_{eff} and $K_{4//}$ in equation (3) are the effective magnetic anisotropy and cubic magnetocrystalline anisotropy, respectively; M_s is the saturated magnetization. In addition, the resonant magnetic field of the uniform precession mode at equilibrium is obtained from the total free energy using the following equation: $(2\pi f/\gamma)^2 = (F_{\theta_M\theta_M}F_{\varphi_M\varphi_M} - F^2{}_{\theta_M\varphi_M})/M_s{}^2\sin^2\theta_M$ [37]. Where f is the microwave frequency, and γ is the gyromagnetic factor. When the high saturated magnetization under a high applied in-plane magnetic field is considered, the magnetic moment of CFA lies in the plane of the film and a coherent rotation of the magnetic moment exists, such that $\theta_M = \pi/2$ and $\varphi_M = \varphi_H$. Therefore, we obtain:

$$\begin{aligned} H_r &= \frac{(2\pi f/\gamma)^2}{4\pi M_s} - \frac{2K_{4//}}{M_s}\cos 4(\varphi_H - a) - \frac{2K_{eff}}{M_s}\cos 2(\varphi_H - b) \\ &= H_{r0} - H_{4//}\cos 4(\varphi_H - a) - H_{eff}\cos 2(\varphi_H - b) \end{aligned} \tag{4}$$

the angles a and b represent the initial positions of the axes of the cubic magnetocrystalline anisotropy and effective magnetic anisotropy, respectively, with respect to the starting point used in our measurements. The effective anisotropy field is given by $H_{eff} = 2K_{eff}/M_s$, and the in-plane magnetocrystalline anisotropy field is given by $H_{4//} = 2K_{4//}/M_s$. To obtain the change in the value of $H_{4//}$ and H_{eff} with change in the electric fields, the fitting curves of the H_r–φ_H at 480 °C, 520 °C, and 550 °C by equation (4) are shown in figure 4(a). With increasing T_s, $H_{4//}$ is 19.5, 19.0, and 14.0 mT, respectively. Meanwhile, H_{eff} is 3.0, 3.7, and 11.7 mT, respectively. The origin of the decrease of $H_{4//}$ (related to the magnetocrystalline anisotropy energy with four-fold symmetry) can be resulted from the deterioration of $B2$ phase order with increasing T_s, as confirmed by the increasing of the H_{eff} related to the in-plane uniaxial magnetic anisotropy energy and magnetoelastic energy both with two-fold symmetry. The result can be in consistent with that measured by XRD as shown in figure 1(b) and AMR measurement as shown in figures 2(b) and (c).

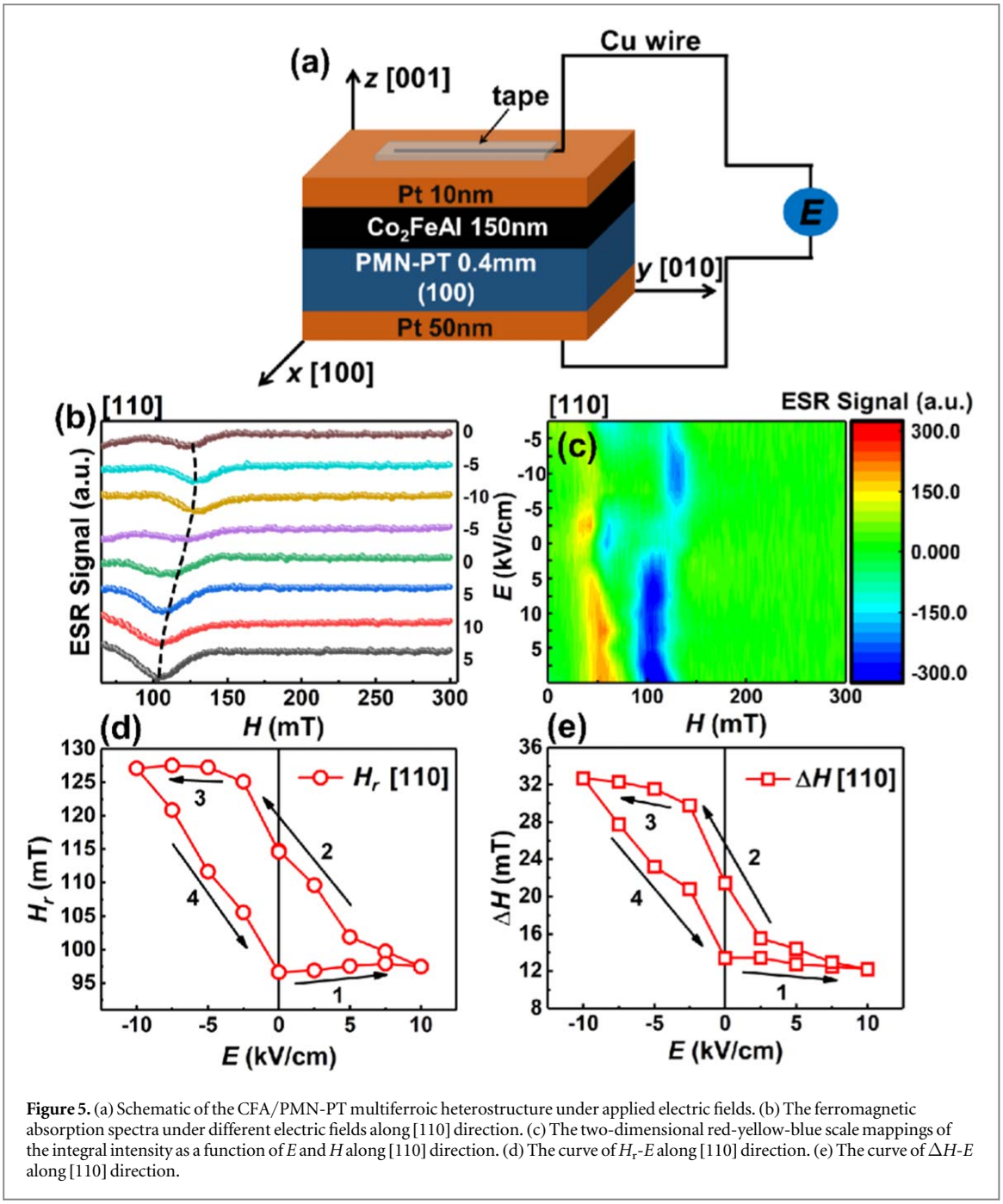

Figure 5. (a) Schematic of the CFA/PMN-PT multiferroic heterostructure under applied electric fields. (b) The ferromagnetic absorption spectra under different electric fields along [110] direction. (c) The two-dimensional red-yellow-blue scale mappings of the integral intensity as a function of E and H along [110] direction. (d) The curve of H_r-E along [110] direction. (e) The curve of ΔH-E along [110] direction.

From the above result, the sample with highest $B2$ phase ordering degree was that at 480 °C. Which was chosen to investigate the ME coupling effect in the Co_2FeAl/PMN-PT heterostructure. The measurement setup was shown in figure 5(a). The FMR spectra of the sample under different applied electric fields (E) along [110] direction were obtained as shown in figure 5(b). E was applied from P_r^-—10 kV cm^{-1}-P_r^+-—10 kV cm^{-1}-P_r^-. P_r^+ refers to the positive remanent polarization state when the electric field was reduced from 10 kV cm^{-1} to 0 kV cm^{-1}. P_r^- represents the negative remanent polarization state when the electric field is changed from −10 kV cm^{-1} to 0 kV cm^{-1}. The two-dimensional red-yellow-blue scale mappings of the integral intensity as a function of E and H were shown in figure 5(c). These integration curves of the FMR spectra were fitted using equation (2), and the related parameters were obtained. H_r had a slight increase when sweeping E from P_r^- to 10 kV cm^{-1}, and decreasing E from 10 to −5 kV cm^{-1}. H_r increases sharply and approximately linearly, while it remained almost unchanged as E was swept from −5 to - −10 kV cm^{-1}, and then H_r decreased sharply and linearly with E changing from −10 kV cm^{-1} to P_r^-. The *loop*-like curve of H_r as a function of E were shown in figure 5(d), which exhibited the non-volatile behavior. The similar phenomenon can be obtained in this curve of ΔH dependence of E as shown in figure 5(e).

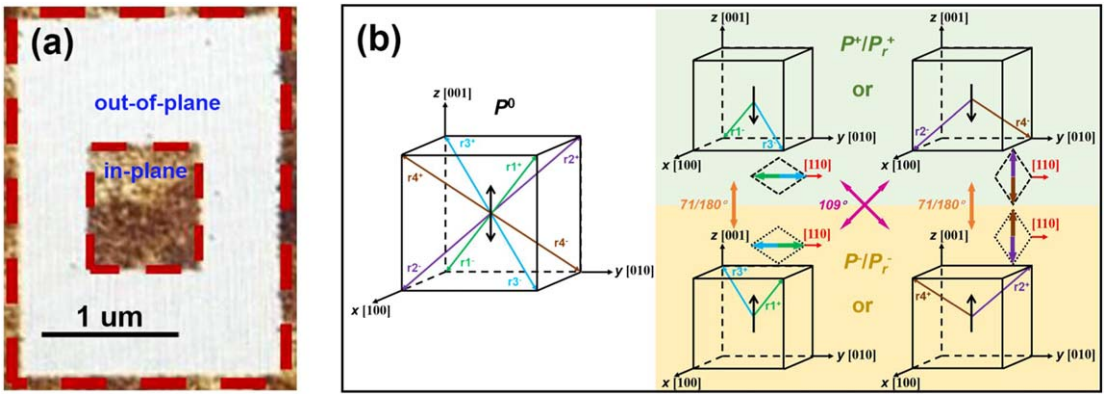

Figure 6. (a) The out-of-plane (white) and in-plane (brown) phase PFM images at P^+. (b) The polarization variants of rhombohedral phase at P^+, P_r^+, P^-, and P_r^-, respectively.

The magnetoelectric coupling effects in FM/FE heterostructure included piezostrain effect and charge effect. Generally, the charge effect will only occur in the thinner FM layer, which can be neglected in this sample (the thickness of CFA ~150 nm). According to our previous reports, the piezostrain effect mediated-the magnetic parameters dependence on the electric field exhibited a butterfly-like behavior. As shown in figures 5(d) and (e), the *loop*-like behavior of $H_r - E$ and $\Delta H - E$ curve implies another type of ME coupling mechanism taken into account in this sample. Zhang *et al* also have reported electric field-mediated *loop*-like magnetization in $Co_{40}Fe_{40}B_{20}$/PMN-PT heterostructure, which can attributed to the combined action of 109° ferroelastic domain switching [22]. In order to further verify the *loop*-like ME coupling behavior in this sample, ferroelectric domains of PMN-PT substrate were measured by PFM. The out-of-plane and in-plane PFM images of PMN-PT substrate at P^+ were shown in figure 6(a). P^+ and P^- are the polarization when applying electric field 10 and −10 kV cm^{-1}. P^0 represents the unpoled state. As shown in figure 6(b), PMN-PT at P^0 is in the rhombohedral phase with eight spontaneous ($r^{1\pm}$, $r^{2\pm}$, $r^{3\pm}$, and $r^{4\pm}$) polarization along the ⟨111⟩ direction. At P^+ as shown in figure 6(a), the out-of-plane image becomes white, which indicated that all the out-of-plane polarization directions are switched upward. Meanwhile, the in-plane image changes to brown, which means the two possible in-plane polarization directions [111]/[−1 − 11] or [−111]/[1 − 11]. As shown in figure 6(b), when the polarity of electric field was changed, the spontaneous polarization can be switched by 71°, 109° and 180°, respectively [25–27]. When polarization variants changed from P^+/P_r^+ to P^-/P_r^- or $P^-/P_r^- \rightarrow P^+/P_r^+$ ($P^+/P_r^+ \leftrightarrow P^-/P_r^-$), corresponding to 71°/180° ferroelectric domain switching. While the 109° ferroelectric domain switch corresponded to $P_r^+/P_r^- \leftrightarrow P^-/P^+$. In this sample, there were not only 71°/180° switching but also 109°switching, which can lead to a *loop*–like behavior of H_r-E and ΔH-E curve.

Conclusion

We report the half-metallic characteristic of Co_2FeAl Huesler alloy films in $Co_2FeAl/Pb(Mg_{1/3}Nb_{2/3})O_3$-$PbTiO_3$ heterostructure by changing substrate temperature during deposition. With substrate temperature decreasing from 550 °C to 480 °C, the evolution of microstructure shows the *B*2 phase ordering degree of Co_2FeAl thin film increase, which can be verified by measurement of anisotropy magnetoresistance and ferromagnetic resonance. Moreover, the *loop*-like curve of resonance-magnetic-field/linewidth versus electric field exhibits the non-volatile behavior, which can be attributed to the 109° ferroelectric domain switching of PMN-PT substrate.

Acknowledgments

This work is supported by the National Natural Science Foundation of China (grants No. 51671099), and the Fundamental Research Funds for the Central Universities (lzujbky-2018-118).

ORCID iDs

Gesang Dunzhu https://orcid.org/0000-0002-4193-7997
Changjun Jiang https://orcid.org/0000-0002-8461-2711

References

[1] Kandpal H C, Fecher G H and Felser C 2007 Calculated electronic and magnetic properties of the half-metallic, transition metal based Heusler compounds *J. Phys. D: Appl. Phys.* **40** 1507

[2] Groot R A D, Mueller F M, Engen P G V and Buschow K H J 1983 New class of materials: half-metallic ferromagnets *Phys. Rev. Lett.* **50** 2024

[3] Sakuraba Y, Hattori M, Oogane M, Ando Y, Kato H, Sakuma A and Miyazaki T 2006 Giant tunneling magnetoresistance in Co_2MnSi/Al-O/Co_2MnSi magnetic tunnel junctions *Appl. Phys. Lett.* **88** 192508

[4] Inomata K, Ikeda N, Tezuka N, Goto R, Sugimoto S, Wojcik M and Jedryka E 2008 Highly spin-polarized materials and devices for spintronics *Sci. Technol. Adv. Mater.* **9** 014101

[5] Webster P J 1969 Heusler alloys *Contemp. Phys.* **6** 10

[6] Bainsla L and Suresh K G 2016 Equiatomic quaternary Heusler alloys: a material perspective for spintronic applications *Appl. Phys. Rev.* **3** 813

[7] Galanakis I, Dederichs P H and Papanikolaou N 2002 Slater-Pauling behavior and origin of the half-metallicity of the full-Heusler alloys *Phys. Rev.* B **66** 174429

[8] Belmeguenai M, Tuzcuoglu H, Gabor M S, Petrisor T Jr, Tiusan C, Zighem F, Chérif S M and Moch P 2014 Co_2FeAl Heusler thin films grown on Si and MgO substrates: annealing temperature effect *J. Appl. Phys.* **115** 043918

[9] Okabayashi J, Sukegawa H, Wen Z, Inomata K and Mitani S 2013 Large anisotropic Fe orbital moments in perpendicularly magnetized Co_2FeAl Heusler alloy thin films revealed by angular-dependent x-ray magnetic circular dichroism *Appl. Phys. Lett.* **103** 721

[10] Chun B S *et al* 2012 Structural and magnetic properties of epitaxial Co_2FeAl films grown on MgO substrates for different growth temperatures *Acta Mater.* **60** 6714

[11] Hentschel T, Jenichen B, Trampert A and Herfort J 2012 Ferromagnetic Heusler alloy Co_2FeSi films on GaAs (110) grown by molecular beam epitaxy *J. Phys. D: Appl. Phys.* **45** 055002

[12] Okamura S, Miyazaki A, Sugimoto S, Tezuka N and Inomata K 2005 Large tunnel magnetoresistance at room temperature with a Co_2FeAl full-Heusler alloy electrode *Appl. Phys. Lett.* **86** 232503

[13] Kokado S, Tsunoda M, Harigaya K and Sakuma A 2012 Anisotropic magnetoresistance effects in Fe, Co, Ni, Fe_4N, and half-metallic ferromagnet: a systematic analysis *J. Phys. Soc. Jpn.* **81** 024705

[14] Kokado S and Tsunoda M 2013 Anisotropic magnetoresistance effect: general expression of AMR ratio and intuitive explanation for sign of AMR ratio *Adv. Mater. Res.* **750** 978–82

[15] Yang F J, Sakuraba Y, Kokado S, Kota Y, Sakuma A and Takanashi K 2012 Anisotropic magnetoresistance in Co_2(Fe, Mn)Si Heusler epitaxial films: a fingerprint of half-metallicity *Phys. Rev.* B **86** 020409 (R)

[16] Eerenstein W, Wiora M, Prieto J L, Scott J F and Mathur N D 2007 Giant sharp and persistent converse magnetoelectric effects in multiferroic epitaxial heterostructures *Nat. Mater.* **6** 348

[17] Wang F L, Zhou C, Zhang C, Dong C H, Yang C C, Jiang C J and Xue D S 2014 Piezoelectric control of magnetic dynamics in Co/Pb$(Mg_{1/3}Nb_{2/3})O_3$-$PbTiO_3$ heterostructure *Appl. Phys. Lett.* **105** 062407

[18] Gueye M, Wague B M, Zighem F, Belmeguenai M, Gabor M S, Petrisor T Jr, Tiusan C, Mercone S and Faurie D 2014 Bending strain-tunable magnetic anisotropy in Co_2FeAl Heusler thin film on Kapton® *Appl. Phys. Lett.* **105** 062409

[19] Thiele C, Dörr K, Bilani O, Rödel J and Schultz L 2007 Influence of strain on the magnetization and magnetoelectric effect in $La_{0.7}A_{0.3}MnO_3$/PMN−PT(001) (A = Sr, Ca) *Phys. Rev.* B **75** 794

[20] Spaldin N A, Cheong S W and Ramesh R 2010 Multiferroics: past, present, and future *Phys. Today* **63** 38

[21] Zhang C, Wang F L, Dong C H, Gao C X, Jia C L, Jiang C J and Xue D S 2015 Electric field mediated non-volatile tuning magnetism at the single-crystalline Fe/Pb$(Mg_{1/3}Nb_{2/3})_{0.7}Ti_{0.3}O_3$ interface *Nanoscale* **7** 4187

[22] Zhang S *et al* 2012 Electric-field control of nonvolatile magnetization in $Co_{40}Fe_{40}B_{20}$/Pb$(Mg_{1/3}Nb_{2/3})_{0.7}Ti_{0.3}O_3$ structure at room temperature *Phys. Rev. Lett.* **108** 137203

[23] Jiang C J, Zhang C, Dong C H, Guo D W and Xue D S 2015 Electric field tuning of non-volatile three-state magnetoelectric memory in FeCo-$NiFe_2O_4$/Pb$(Mg_{1/3}Nb_{2/3})_{0.7}Ti_{0.3}O_3$ heterostructures *Appl. Phys. Lett.* **106** 1240004

[24] Jiang C J, Wang F L, Dong C H, Zhou C, Wu L and Xue D S 2016 A non-volatile four-state magnetic memory in a Co/(011)Pb$(Mg_{1/3}Nb_{2/3})O_3$-$PbTiO_3$ heterostructure *Appl. Phys. Lett.* **108** 71

[25] Zhou C, Dunzhu G S, Yao J L and Jiang C J 2017 Piezostrain control of magnetic anisotropy in Co_2FeAl/Pb$(Mg_{1/3}Nb_{2/3})O_3$-30%$PbTiO_3$ heterostructure *J. Alloy. Compd.* **710** 680–4

[26] Zhou C, Wang F L, Dunzhu G S, Yao J L and Jiang C J 2016 Piezostrain tuning non-volatile 90° magnetic easy axis rotation in Co_2FeAl Heusler alloy film grown on Pb$(Mg_{1/3}Nb_{2/3})O_3$-$PbTiO_3$ heterostructures *J. Phys. D: Appl. Phys.* **49** 455001 (6pp)

[27] Noheda B, Cox D E, Shirane G, Gao J and Ye Z G 2002 Phase diagram of the ferroelectric relaxor (1-x)$PbMg_{1/3}Nb_{2/3}O_3$-x$PbTiO_3$ *Phys. Rev.* B **66** 054104

[28] Baek S H *et al* 2010 Ferroelastic switching for nanoscale non-volatile magnetoelectric devices *Nat. Mater.* **9** 309

[29] Fu H X and Cohen R E 2000 Polarization rotation mechanism for ultrahigh electromechanical response in single-crystal piezoelectrics *Nat.* **403** 281

[30] Buschow K H J and Engen P G V 1981 Magnetic and magneto-optical properties of Heusler alloys based on aluminium and gallium *J. Magn. Magn. Mater.* **25** 90

[31] Gabor M S, Petrisor T Jr, Tiusan C, Hehn M and Petrisor T 2011 Magnetic and structural anisotropies of Co_2FeAl Heusler alloy epitaxial thin films *Phys. Rev.* B **84** 134413

[32] Okamura S, Miyazaki A, Tezuka N, Sugimoto S and Inomata K 2006 Epitaxial growth of ordered $Co_2(Cr_{1-x}Fe_x)Al$ full-Heusler alloy films on single crystal substrates *Mater. Trans.* **47** 15

[33] Yang F J, Wei C and Chen X Q 2013 Half-metallicity and anisotropic magnetoresistance of epitaxial Co_2FeSi Heusler films *Appl. Phys. Lett.* **102** 172403

[34] Farle M 1998 Ferromagnetic resonance of ultrathin metallic layers *Rep. Prog. Phys.* **61** 755

[35] Zhou C, Shen L K, Liu M, Gao C X, Jia C L and Jiang C J 2018 Strong nonvolatile magnon-driven magnetoelectric coupling in single-crystal Co/$[PbMg_{1/3}Nb_{2/3}O_3]_{0.71}[PbTiO_3]_{0.29}$ heterostructures *Phys. Rev. Appl.* **9** 014006

[36] Stoner E C and Wohlfarth E P 1948 A mechanism of magnetic hysteresis in heterogeneous alloys *Philos. Trans. R. Soc. London, Ser.* A **240** 599

[37] Lenz K, Kosubek E, Baberschke K, Wende H, Herfort J, Schönherr H P and Ploog K H 2005 Magnetic properties of Fe_3Si/GaAs(001) hybrid structures *Phys. Rev.* B **72** 144411